Journal of Applied Polymer Science

# Carbon Nanomaterial-Based Copolymer of Styrene–Divinylbenzene Resins: Efficient Interaction Through Graphene/CNTs Polymer Network

**Yanan Li, Fengping Yu, Wenjun He, Weimin Yang**
SINOPEC Shanghai Research Institute of Petrochemical Technology, Shanghai 201208, People's Republic of China
Correspondence to: W. Yang (E-mail: yangwm.sshy@sinopec.com)

**ABSTRACT:** Carbon nanotubes (CNTs) and graphene were separately incorporated into the cross-linked network of styrene–divinylbenzene composites via *in situ* suspension polymerization. The prepared copolymers were first chloromethylated and then aminated with trimethylamine to obtain ion exchange resins (IERs). The CNTs-based and graphene-based composites exhibited good dispersion throughout the polymer matrix with strong interaction within the network. Remarkable enhancement in antiswelling properties and thermal stabilities confirmed that graphene showed better compatibility and stronger interfacial adhesion than CNTs. The structural and thermal properties of the CNTs-based and graphene-based IERs were also significantly improved even at low loadings of 0.4 wt % compared with those when no CNTs and graphene were added. © 2014 Wiley Periodicals, Inc. J. Appl. Polym. Sci. **2015**, *132*, 41234.

**KEYWORDS:** composites; nanostructured polymers; resins; structure–property relations; thermal properties

Received 15 April 2014; accepted 29 June 2014
**DOI: 10.1002/app.41234**

## INTRODUCTION

Various carbon nanomaterials including fullerene, single/multiwall carbon nanotubes (CNTs), and graphene have attracted considerable attention in recent years because of their extraordinary mechanical, electrical, and thermal properties.[1–3] Among them, CNTs and graphene are the representative ones with one and two-dimensional nanostructure for prospective applications in solar cells, supercapacitors, batteries, and polymer nanocomposites.[4–7] Attention in polymer research in the past two decades has also been focused on the development of nanocomposites to enhance multifunctional properties of neat polymeric matrices using carbon nanomaterial reinforcements, which strongly depend on the good dispersion of nanofillers and interfacial action within the polymeric matrix.

Different techniques have been developed to achieve good dispersion, including surfactant stabilized mixing, emulsion polymerization, solvent-based exfoliation, and sonication-induced polymerization.[8–11] Generally, the chemical functionalized carbon materials are considered to be promising reinforcing materials for polymer composite, such as polymer-grafted CNTs/graphene and graphene oxide.[11–14] Among these items, CNTs were the most popular material for fabricating the composites. He et al. reported that the functionalized CNTs–polystyrene composites were synthesized by nitroxide mediated polymerization.[15] Lagoudas et al. found a similar percolation threshold in the prepared CNTs/epoxy composites, and the thermal conductivity of the composites was increased by 5.5% with the electrical conductivity increased by 10 orders of magnitude.[16] It has been demonstrated that graphene oxide (GO) could be stably dispersed in the emulsion or microemulsion polymerization.[17,18] However, polymer/GO composites were hardly formed when GO was added to the monomer solution. Additional reduction step was required using hydrazine as chemical reducing agent in the multistep procedure.

Herein, we report a novel method for the synthesis of carbon nanomaterial-based copolymer of styrene–divinylbenzene composite using *in situ* suspension polymerization without any surfactant. The composites are prepared by solution-phase premixing of CNTs or graphene in styrene monomer, followed by the *in situ* suspension polymerization. Obtained composites should be compatible with the polymer matrix to avoid the agglomeration of carbon nanomaterials and potential microscopic phase separation in the composites. Furthermore, due to the good dispersion of carbon nanomaterials, CNTs/graphene were involved in forming a continuous polymer network with strong interaction within the surrounding polymer matrix. Meanwhile, the prepared ion exchange resins (IERs) composites with subsequent chloromethylation and amination steps showed enhanced structural and thermal stability compared to the conventional IER even at extremely low graphene loadings of 0.4 wt %.

## EXPERIMENTAL

### Materials

Styrene (Sinopharm Chemical Reagent, 99%) and DVB (Sigma-Aldrich Chemicals, technical grade, 80%) were washed by

NaOH solution (5 wt %) thrice to remove inhibitors, then washed again with deionized water, stirred over magnesium sulfate overnight and then over calcium hydride, distilled, and stored under nitrogen atmosphere at 4°C. The purification of radical initiator benzoyl peroxide (BPO, Sinopharm Chemical Reagent, 98%) was carried out by recrystallization from methanol solution. Chloromethyl ethylether (96%) was purchased from Tokyo Chemical Industry. Other chemicals, including gelatin (CP), zinc chloride ($ZnCl_2$, AR), tetrahydrofuran (THF, AR), trimethylamine hydrochloride (98%), and 1,2-dichloroethane (99%) were purchased from Sinopharm Chemical Reagent, and were used as received. Pristine CNTs (JCMT-90, 90%) and graphene (JCGNP-15-10, 99.5%) were purchased from Nanjing JCNANO Technology, which were calcined to remove amorphous carbon at 110°C for 1 h in air.

### Synthesis of the CNTs-Based and Graphene-Based IER Composites

CNTs or graphene were suspended in 10 mL styrene monomer, and then ultrasonicated for 10 min to obtain the required dispersions. Then 2.5 g gelatin were dissolved in 200 mL deionized water at 40°C. The monomer mixture consisted of 45.3 g styrene, 4.4 g DVB, and 0.5 g BPO. The suspension polymerization was carried out in the presence of CNTs and graphene separately at the organic-aqueous interface with whole-process stirring in a 500 mL round-bottom flask. After 30 min preblending at 40°C, raised temperature gradually to 70°C, and maintained for 1 h. The polymerization occurred and proceeded at 80–83°C for 6 h and then at 95–97°C for 4 h. The 0.4 wt % CNTP and GEP composites precipitated out as beads, which was then separated and washed by hot deionized water. The obtained composites were dried at 90°C and designated as 0.4-CNTP and 0.4-GEP.

Styrene–divinylbenzene crosslinked copolymer beads were also synthesized with the same reagents and condition except the addition of graphene for comparison. The polymer was designated as PS-DVB.

The Friedel–Craft reaction was used to introduce chloromethyl groups to the crosslinking network of the polymer composites. The composite (25.0 g) and chloromethyl ethylether (75 mL) were mixed to swell the cross-linked polymer for 2 h at room temperature. Then, $ZnCl_2$ (9.6 g) was added to the mixture in two batches. The reaction was allowed to proceed at 38–40°C for 10 h. The chloromethylation products were washed by acetone and dried until a constant weight was reached.

The chloromethylation products (designated as 0.4-CNTP-Cl, 0.4-GEP-Cl, and PS-DVB-Cl) were immersed in 1,2-dichloroethane to swell for 2 h. Trimethylamine hydrochloride was added to the resulting products in three batches and the reaction ran for 6 h at 30°C. After the reaction, the mixture was diluted with deionized water and NaOH solution in sequence. The final products were dried at 50°C until a constant weight was reached. Schematic diagram of reaction steps involved in the preparation of CNTs-based and graphene-based composites is demonstrated in Scheme 1.

CNTs-based and graphene-based composites IER and PS-DVB IER in hydroxylic form obtained after amination reactions were designated as 0.4-CNTP-OH, 0.4-GEP-OH, and PS-DVB-OH, respectively. In this study, all the copolymers with a crosslinking density (CD) of 6% were controlled and presented according to the following equation.[19]

$$\mathrm{CD}\ (\%) = \frac{m(\mathrm{DVB})}{m(\mathrm{DVB}) + m(\mathrm{St})} \times 100\% \quad (1)$$

### Characterizations and Measurements

Scanning electron microscopy (SEM, Philips XL30E) was used to observe the general size and morphology of the polymer beads. The polymer composites bead samples were coated with a thin layer of gold on the surface. The pressure during scanning was $5.2 \times 10^{-9}$ MPa and the accelerated voltage was 5 kV.

The Raman spectra were collected with LabRam-1B micro-Raman spectrometer (Jobin Yvon Instrument), using the He–Ne laser excitation line at 632.8 nm. Acquisition time was 30 s with a final laser power of about 3 mW at the sample surface.

The X-ray diffraction (XRD) measurements were performed on a Bruker D8 Advanced Diffractometer equipped with Cu K$\alpha$ radiation ($\lambda = 0.154$ nm, 40 kV, 40 mA) at a scanning rate of 0.4°/min within a $2\theta$ range of 5°–80°.

The functional groups were examined by Fourier transformed infrared (FTIR) spectrum using a Nicolet 5700 spectrometer (ThermoElectron, Madison, WI). The sample was pulverized and then diluted in dried KBr to obtain a homogeneous mixture with a 1 : 49 sample-to-KBr ratio. The spectra were recorded from KBr pellets at a range of 4000–400 $cm^{-1}$ with 32 scans and a resolution of 4 $cm^{-1}$ by subtracting the background spectrum from subsequent spectra, and such difference spectra are reported herein.

Thermo-gravimetric analyses (TGA) were performed on a TA Instruments SDT Q600 TGA thermo-gravimetric analyzer from room temperature to 900°C at a heating rate of 10°C/min under a dynamic (100 mL/min) air atmosphere. The differential scanning calorimetry (DSC) cycling curves were measured with DSC Q2000 (TA Instruments-Waters LLC). The procedures of each DSC run were as follows: heat from room temperature to 200°C, then hold isothermal at 200°C for 5 min, cooling equilibrated to 50°C, and then heat from 50 to 160°C. Samples of approximately 7–9 mg in these examination were weighed with a precision of 0.01 mg aluminum pans prior to analysis. The temperature scanning rate for all cycles was 10°C/min in 50 mL/min $N_2$ as the purge gas. All the measurements were repeated at least three times.

The swelling properties were determined through the procedures given below. The polymer was immersed in the deionized water for 24 h and dried at 60°C for 72 h. The volume was measured and recorded before and after the drying process as $V_A$ and $V_B$, respectively. Besides, the polymer was immersed in deionized water, NaOH solution (1 mol/L) and tetrahydrofuran (THF) for 24 h, then the volume was recorded as $V_s$. The dry resin volume ($V_{\mathrm{dry}}$) and swelling capacity in the solution (SR) of the polymer beads were calculated as follow equations:[20]

$$V_{\mathrm{dry}} = \frac{V_{0\mathrm{M}}}{V_B} \times V_A \quad (2)$$

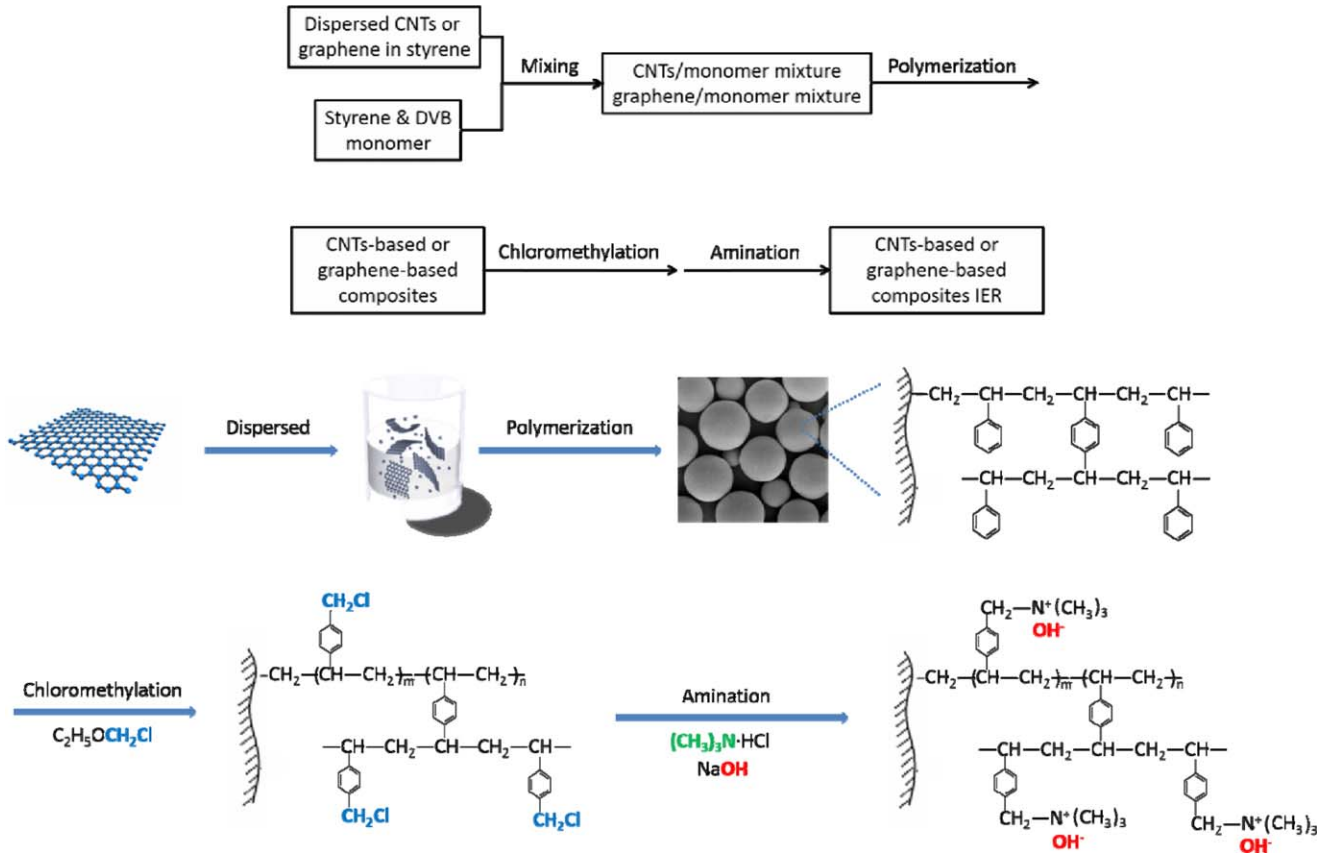


**Scheme 1.** Schematic diagram of reaction steps involved in the preparation of CNTs-based and graphene-based composites. [Color figure can be viewed in the online issue, which is available at wileyonlinelibrary.com.]

$$\mathrm{SR}\ (\%) = \frac{V_s - V_{\mathrm{dry}}}{V_{\mathrm{dry}}} \times 100\% \tag{3}$$

For evaluating the catalytic performance of the resins, total ion-exchange capacity (IEC) was measured according to National Standard of People's Republic of China GB/T 5760-2000, which describes the determination of the exchange capacity of anion-exchange resins in hydroxylic form.[21] The methodology was as follows: the sample was first pretreated according to National Standard of People's Republic of China GB/T 5476. Then, it was washed with HCl aqueous solution (2 mol/L), deionized water, and NaOH aqueous solution (2 mol/L) in sequence. The prepared sample was measured and soaked in 100 mL standard HCl solution at 40°C for 2 h, than 25 mL soaked solution was subsequently titrated with standard NaOH solution using phenolphthalein as the indicator. The IEC ($Q$, mmol/g) was calculated according to Eq. (4).

$$Q = \frac{100c_1 - 4c_2V_t}{W(1-A)} \tag{4}$$

where $c_1$ is the molar concentration of standard HCl solution, $c_2$ is the molar concentration of standard NaOH solution. The volume of the titrating solution of NaOH was recorded as $V_t$, while $W$ is the weight of the prepared IER samples. $A$ is the moisture content of the IER sample measured by National Standard of People's Republic of China GB/T 5759-2000.

## RESULTS AND DISCUSSION

### Morphology of PS-DVB, CNTs-Based and Graphene-Based Nanocomposites

The CNTs-based and graphene-based nanocomposites were prepared separately via a modified surfactant-free *in situ* suspension polymerization of styrene, divinylbenzene, and carbon nanomaterials. The quality of the carbon nanomaterials dispersion in the monomer before polymerization not only affects the further dispersion in the polymer matrix, but also directly correlates with their effectiveness for improving thermal, antiswelling, and other properties. The dispersion stability against van der Waals aggregation of CNTs and graphene in deionized water and styrene monomer were compared in Figure 1. Figure 1(A) shows the vials containing CNTs or graphene at a concentration of 0.1 mg/mL after 10 min ultrasonication immediately, and Figure 1(B) shows the photos of the vials standing for 24 h. Although some particulates in the graphene suspensions settled at the bottom of the vials over 24 h, it still appears that graphene shows better dispersion behavior than CNTs. Moreover, in the styrene suspension, graphene stayed homogenous at least for 12 h. The probability of such enhanced dispersion of graphene could result in high stability, and the equilibrium aggregation of the materials would be also reduced. The highly stable graphene suspension in monomer is possibly due to strong interactions between graphene and monomer, thus favoring the homogeneity of the beads during the suspension polymerization.

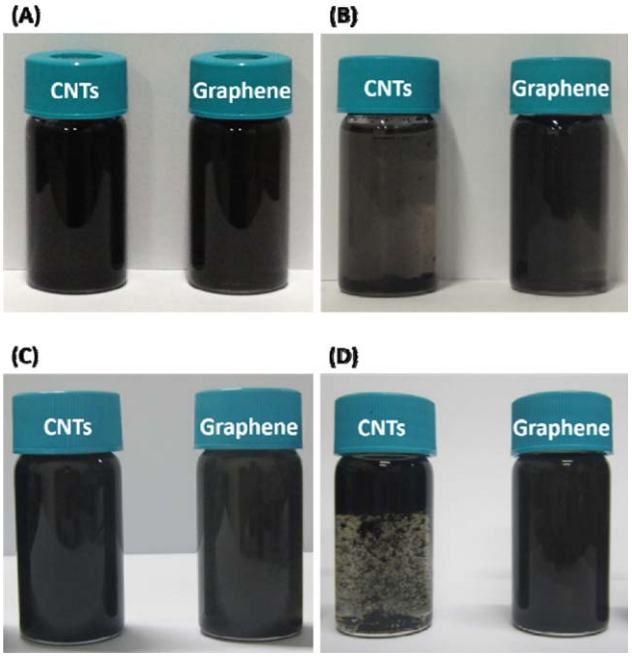


**Figure 1.** Photographs of (A) CNTs and graphene dispersions in deionized water with 10 min ultrasonication and (B) then photographed after 24 h; (C) CNTs and graphene dispersions in styrene with 10 min ultrasonication, and (D) then photographed after 24 h. All with [CNTs] = 0.1 mg/mL or [graphene] = 0.1 mg/mL. [Color figure can be viewed in the online issue, which is available at wileyonlinelibrary.com.]

Figure 2 presents the SEM micrographs of the CNTP IER, GEP IER, and PS-DVB IER in chloric and hydroxylic form. The good dispersion of graphene in the solution was retained in the polymer composites. By suspension polymerization, graphene was proximately homogeneous dispersing in the monomer and bound in polymer crosslinked structure gradually with the elevated temperature. Therefore, the graphene-based nanocomposites resulted in very fine beads with resembling bare PS-DVB system, and the size of the beads was in the same range of 400–600 $\mu$m. Comparing the SEM images, the surface morphology of the as-prepared IER beads clearly shows the graphene-based polymer beads could be more effectively to form into spherical shape with much smoother surface than CNTs-based polymer beads during the polymerization. This visual effect is due to different dispersion of CNTs and graphene in the polymer matrix. CNTs facilitate aggregation in bundles, leading to poor and inhomogeneous distribution in the polymer and a limited interfacial adhesion between the CNTs and the polymer.

**Properties of PS-DVB, CNTs-Based and Graphene-Based IER**

The Raman spectra of CNTs, graphene, PS-DVB, CNTs-based and graphene-based composites are plotted in Figure 3. Typically, Raman spectroscopy is the state of art to investigate the structure defects in CNTs and graphene by monitoring the D- and G-band.[22] The D-peak, which occurs at ~1350 $cm^{-1}$, is the finger print of defects since it is associated with hexagonal framework defects or $sp^3$ carbon, while the G-peak at ~1580 $cm^{-1}$ is due to the inplane bond stretching motion of $sp^2$ carbon. Besides, the spectra also exhibit another characteristic peak appeared at ~2680 $cm^{-1}$ (2D-band). All the recorded spectra were fitted using Lorentzian lineshapes and the intensity ratios of $D/G$ were calculated from the fitted curve parameter.[22–25]

As shown in Figure 3, the composites display the prominent peaks at ~1350, ~1580, and 2680 $cm^{-1}$ with some characteristic

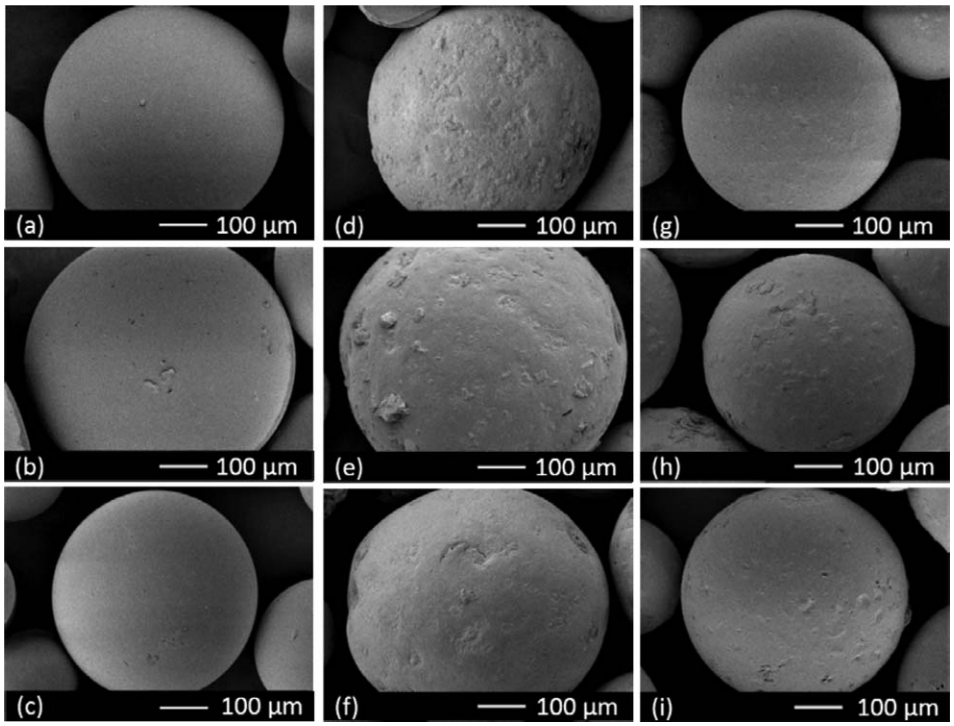


**Figure 2.** SEM photos of PS-DVB and nanocomposites beads: (a) PS-DVB; (b) PS-DVB-Cl; (c) PS-DVB-OH; (d) 0.4-CNTP; (e) 0.4-CNTP-Cl; (f) 0.4-CNTP-OH; (g) 0.4-GEP; (h) 0.4-GEP-Cl; (i) 0.4-GEP-OH.

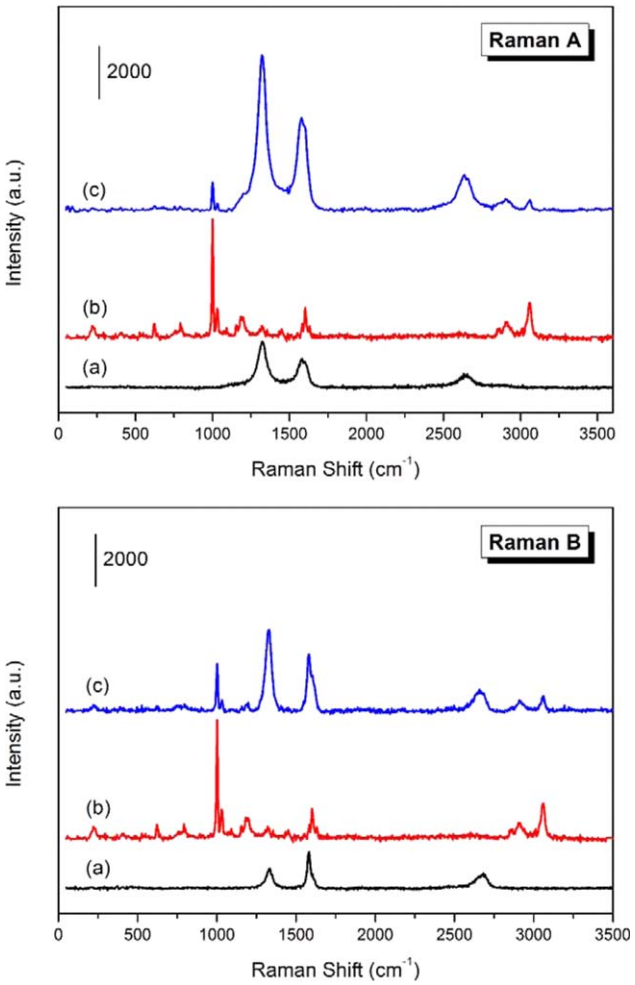


**Figure 3.** Raman spectra of pristine CNTs, pristine graphene, PS-DVB and nanocomposites: (A), (a) pristine CNTs, (b) PS-DVB, (c) 0.4-CNTP; (B), (a) pristine graphene, (b) PS-DVB, (c) 0.4-GEP. [Color figure can be viewed in the online issue, which is available at wileyonlinelibrary.com.]

peaks of the polymer structure. Since the $I_D/I_G$ ratio is 1.59 for pristine CNTs and 0.84 for pristine graphene, the *D*/*G* intensity ratio increases apparently from pristine graphene to the graphene-based composite ($I_D/I_G$ : 1.62), suggesting a carbon transformation of $sp^2$-domain to $sp^3$-domain and formation of covalent bonds between polymer and graphene induced by polymerization.[26,27] In Figure 3(B), the 0.4-GEP composite shows a G-peak shift from 1578 to 1581 $cm^{-1}$, indicating the electron transfer from graphene to the polymer chains with strong interactions.[28] It can be assumed that during the suspension polymerization of 0.4-GEP, graphene could effectively tether with the polymer chain radicals or initiator fragments and penetrate into the polymer network,[21,29] which leads to well dispersion in the polymer matrix and enhanced interaction between the graphene and the polymer network. With comparison of 0.4-CNTP ($I_D/I_G$ : 1.58) and 0.4-GEP composites, the Raman spectra confirm that graphene enable the stronger chemical interaction within the polymer matrix than CNTs.

From the XRD patterns in Figure 4, PS-DVB shows broad peaks at ~9.2° and 19.0°, revealing its amorphous feature of the

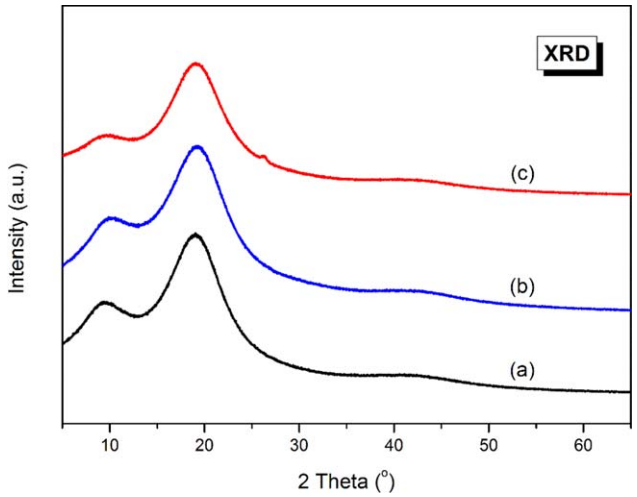


**Figure 4.** XRD patterns of (a) PS-DVB, (b) 0.4-CNTP, (c) 0.4-GEP. [Color figure can be viewed in the online issue, which is available at wileyonlinelibrary.com.]

crosslinked polymer matrix. For comparison, the 0.4-CNTP and 0.4-GEP composites present the similar XRD patterns as that of PS-DVB, indicating the good dispersion of CNTs or graphene sheets in the polymer matrix. However, the center position of the peaks shift up and the peaks become wide and weak, apparently it could be due to the interaction between the polymer chains and carbon nanomaterials,[30] which is in line with the Raman results.

FTIR spectroscopy is performed on the crosslinked, chloromethylated, and aminated polymer samples, shown in Figure 5. The overall spectra for the CNTs-based and graphene-based composites were quite similar. After chloromethylation, the samples showed the absorption peaks at 1265 and 676 $cm^{-1}$, which were attributed to the inplane bending vibration of aromatic C–H in Ph–$CH_2$Cl groups and C–Cl stretching vibration.[15] Concomitantly, the weak shoulder peaks at ~1421 $cm^{-1}$ were assigned to the bending vibration of C–H in chloromethyl (–$CH_2$Cl) groups. After amination, all the chlorine-containing groups disappeared and new peaks at ~976 $cm^{-1}$ attributed to C–N stretching were clearly observed. Besides, the peaks at ~1630 $cm^{-1}$ corresponds to O–H inplane bending vibration. All these results confirmed the existence of $-N^+(CH_3)_3OH^-$ groups grafted on the polymer chains in successful chloromethylation and amination step.[21,31–33]

To the authors' knowledge, some studies have focused on the nonoxidative stability (in $N_2$ or Ar) and comparatively little data exists on the oxidative stability of the carbon nanomaterials composites. In this study, TGA was performed in air on the CNTs, graphene, PS-DVB, CNTs-based and graphene-based composites to study the degradation process of the composites, as well as to determine the effects of CNTs and graphene on the thermal stability of the composites.

As illustrated in Figure 6, PS-DVB sample exhibits three degradation steps occurring at 100–200, 200–400, and 400–600°C, respectively. The initial 6% weight loss was due to the elimination of the moisture in the samples at the first stage. Then the

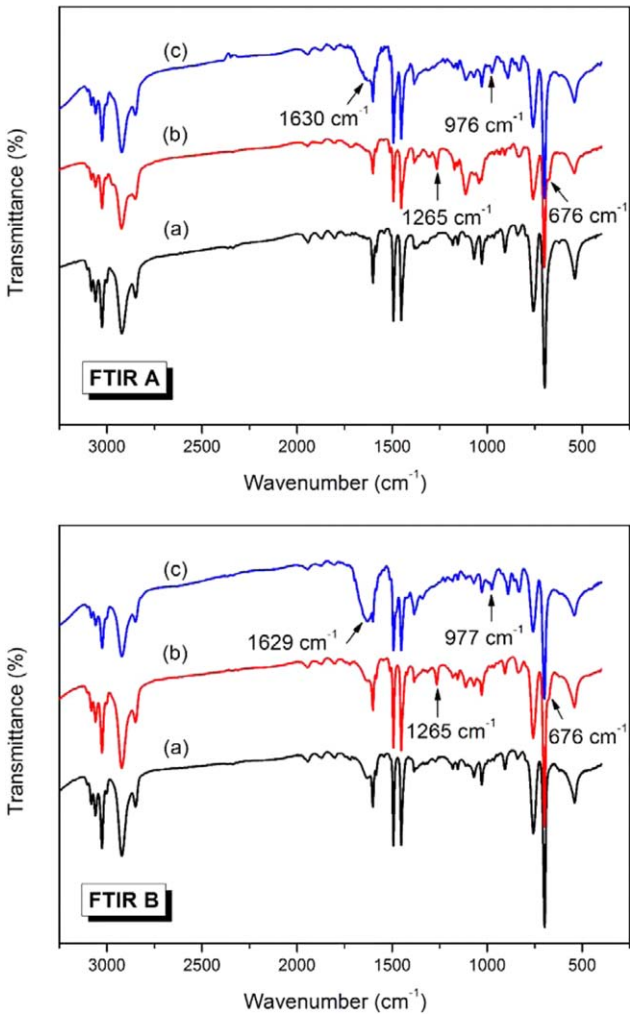


**Figure 5.** FTIR spectra of the nanocomposites: (A), (a) 0.4-CNTP, (b) 0.4-CNTP-Cl, (c) 0.4-CNTP-OH; (B), (a) 0.4-GEP, (b) 0.4-GEP-Cl, (c) 0.4-GEP-OH. [Color figure can be viewed in the online issue, which is available at wileyonlinelibrary.com.]

major stage of weight loss about 85%, occurring at ~210°C, corresponding to the branching chains and crosslinking network degradation to short chains or volatile compounds induced by oxidative atmosphere.[34,35] At the third degradation stage, about 9%, which could be assigned to the combustion of char residue of carbonaceous to volatile fragments (such as carbon dioxide and steam), and all the samples completely burn off at 600°C. In the case of composites, the last stage showed higher amount of char residue compared to PS-DVB, which is related to the decomposition/combustion of the residue of carbonaceous and CNTs/graphene.

Table I lists the results of the extrapolated degradation on set temperatures ($T_{deg}$) and the temperatures at the maximum weight loss velocity of the DTA curves ($T_{max1}$ and $T_{max2}$). PS-DVB reached the maximum weight loss velocity at 409.8°C, which was the lowest value of all the samples. The $T_{deg}$ and $T_{max}$ of the composites all shifted to higher temperature, especially for the 0.4 wt % graphene-based composites, it increased by ~15°C compared to the PS-DVB and PS-DVB-OH. This

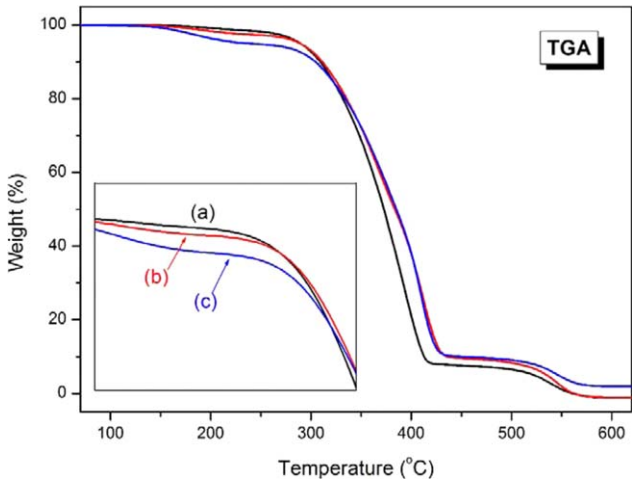


**Figure 6.** TGA curves of PS-DVB and nanocomposites: (a) PS-DVB, (b) 0.4-CNTP, (c) 0.4-GEP. [Color figure can be viewed in the online issue, which is available at wileyonlinelibrary.com.]

indicates that the thermal stability of the conventional PS-DVB IER composite was improved by the addition of carbon nanomaterials.

A thermal transition of a segmental motion of the polymer chains was examined and the glass transition temperature ($T_g$) obtained by DSC measurement were also summarized in Table I. In the case of PS-DVB, $T_g$ was at 110.3°C and slightly increased by 1°C for the composites.

In an attempt to study the influence of CNTs and graphene over the composites, the physical properties of the composites prepared were also listed in Table II. To determine the values of the moisture content, total exchange capacity and swelling capacity, all the samples were measured at least twice. The data show that the basic properties of CNTs-based and graphene-based IER composites resemble the PS-DVB-OH, including particle density, mean particle size, moisture content, total exchange capacity, and swelling capacity. The SR (%) clearly shows the influence of the carbon nanomaterials in the polymer resins on the swelling properties. PS-DVB-OH resin beads swollen greatly in the different solutions and to a less extent of graphene-based resin, while CNTs-based composite shows quite similar value to the neat polymer resin. In particular, it was

**Table I.** Thermal Properties of the IER Samples

| Sample | $T_{deg}$ (°C)[a] | $T_{max1}$ (°C)[b] | $T_{max2}$ (°C)[b] | $T_g$ (°C)[c] |
|---|---|---|---|---|
| PS-DVB | 339.2 | 409.8 | 545.3 | 110.3 |
| 0.4-CNTP | 347.5 | 419.4 | 544.6 | 111.2 |
| 0.4-GEP | 356.9 | 432.5 | 545.5 | 110.9 |
| PS-DVB-OH | 352.8 | 415.7 | 548.0 | 88.8 |
| 0.4-CNTP-OH | 352.0 | 429.3 | 551.7 | 91.2 |
| 0.4-GEP-OH | 372.3 | 431.3 | 549.7 | 91.3 |

[a] Determined by the extrapolated onset temperatures.
[b] Maximum weight loss temperatures in DTA curves.
[c] Determined as the midpoint temperature at half the complete change of heat capacity in DSC curves.

**Table II.** Physical and Chemical Properties of the IER Samples

| Sample | $\rho$ (g/cm$^3$)[a] | $d_v$ (mm)[b] | A (%) | Q (mmol/g) | SR (%) | | |
|---|---|---|---|---|---|---|---|
| | | | | | Water | NaOH (aq) | THF |
| PS-DVB | 0.60 | 0.44 | 21.5±0.1 | 0.28 | 28.1 | 29.2 | 30.5 |
| 0.4-CNTP-OH | 0.61 | 0.48 | 40.9±0.1 | 1.44 | 29.0 | 26.8 | 30.3 |
| 0.4-GEP-OH | 0.65 | 0.54 | 39.8±0.2 | 1.91 | 19.3 | 24.1 | 27.0 |

[a] Mean particle density.
[b] Volume-weighted mean particle size.

found that small amounts of graphene dramatically improve the total exchange capacity behavior. This result could be explained by the fact that the high level electron cloud density of aromatic structure of graphene might favor the electrophilic substitution reaction of chloromethylation process, providing more reactive sites for amination, as shown in Scheme 1.

Hence, the carbon nanomaterials-based polymer resins were successfully synthesized via *in situ* suspension polymerization. The incorporation of CNTs or graphene into the polymer crosslinked networks is beneficial to improve the thermal stability, antiswelling properties of the composites. Generally, "grafting-from", and "grafting-to" approaches have been used to introduce covalent bonds between the CNTs/graphene and polymers.[18,36] For the "grafting-from" methodology, the initiator BPO usually generates phenyl radicals, which can react with the CNTs/graphene and functionalize the graphene sheet. The resulting radical CNTs/graphene species could subsequently react with a monomer molecule and damage the perfect $sp^2$ carbon structure.[29,37–39] Thereby the polymeric fragment is propagated from the CNTs or graphene surface by capturing more and more styrene molecules. After covalent bonding with styrene, a portion of the $sp^2$ carbon on CNTs or graphene is converted to $sp^3$ carbon, which is consistent with the Raman results. Based on the "grafting-to" methodology, the polymer chain with free radical, like .–CH(Ph)-CH$_2$· can be directly conjugated with the CNTs or graphene. The growing polymer chains will terminate through combining with another propagating polymer chain or radical functionalized CNTs/graphene. Besides, the polymer chain might be react with the CNTs/graphene to functionalize the CNTs/graphene with a radical on the surface and allow further conjugation of a new monomer molecule or polymer chain.

The polymer chains incorporate with the CNTs/graphene either by grafting-from or grafting-to methodology. In addition, CNTs and graphene act as covalent crosslinkers to form the polymer network for improved interfacial interaction between carbon nanomaterials and polymer chains. Moreover, the dispersed CNTs or graphene could induce the barrier labyrinth effect, impeding the transport of degradation products of polymer into the gas phase. The heat is required to break the covalent linkages and transport the degradation products of polymer, which tended to shift the $T_{deg}$, $T_{max1}$, and $T_{max2}$ to higher temperatures. As described above, CNTs and graphene could induce the steric limitation through the resin and restricts the polymer chain mobility in the nanocomposite, resulting a higher $T_g$ value.[39,40] Fundamentally, the addition CNTs and graphene could effectively protect against thermal degradation and transition for the polymer network, leading to the enhanced properties of the IER composites.

## CONCLUSIONS

We have demonstrated a novel method for the preparation of CNTs-based and graphene-based copolymer of styrene-divinylbenzene resin composites using a modified surfactant-free *in situ* suspension polymerization. The CNTs and graphene in the composites dispersed well throughout the polymer matrix, which could effectively enhance the electron transfer from CNTs/graphene to the polymer chains with strong interactions. The structural and thermal stability of the copolymers and ion exchange resins were improved with the incorporation of CNTs/graphene in the composites at extremely low loading of 0.4 wt %, which has not been reported. What is more, graphene shows better dispersion and stronger interfacial adhesion than CNTs, which indicates that graphene is much efficient as reinforcement than CNTs in the polymer matrix. This is beneficial in terms of stabilizing the polymer resins at higher temperature and improving the antiswelling properties, which allows a larger window for the systematic study on the IER application in the future.

## ACKNOWLEDGMENTS

This work was sponsored by Science and Technology Commission of Shanghai Municipality, China (13R21421900).

## REFERENCES

1. Aboutalebi, S. H.; Jalili, R.; Esrafilzadeh, D.; Salari, M.; Gholamvand, Z.; Aminorroaya Yamini, S.; Konstantinov, K.; Shepherd, R. L.; Chen, J.; Moulton, S. E.; Innis, P. C.; Minett, A. I.; Razal, J. M.; Wallace, G. G. *ACS Nano* **2014**, *8*, 2456.
2. Keeley, G. P.; McEvoy, N.; Nolan, H.; Holzinger, M.; Cosnier, S.; Duesberg, G. S. *Chem. Mater.* **2014**, *26*, 1807.
3. Wang, H.; Kakade, B. A.; Tamaki, T.; Yamaguchi, T. *J. Power Sources* **2014**, *260*, 338.
4. Al-Youbi, A. O.; Gómez de la Fuente, J. L.; Pérez-Alonso, F. J.; Obaid, A. Y.; Fierro, J. L. G.; Peña, M. A.; Abdel Salam, M.; Rojas, S. *Appl. Catal. B* **2014**, *150–151*, 21.

5. Corso, B. L.; Perez, I.; Sheps, T.; Sims, P. C.; Gül, O. T.; Collins, P. G. *Nano Lett.* **2014**, *14*, 1329.
6. Prasad, K. P.; Chen, Y.; Chen, P. *ACS Appl. Mater. Interfaces* **2014**, *6*, 3387.
7. Sevilla, M.; Yu, L.; Zhao, L.; Ania, C. O.; Titiricic, M.-M. *ACS Sustain. Chem. Eng.* **2014**, *2*, 1049.
8. Das, S.; Wajid, A. S.; Shelburne, J. L.; Liao, Y.-C.; Green, M. *J. ACS Appl. Mater. Interfaces* **2011**, *3*, 1844.
9. Tung, W.-S.; Bird, V.; Composto, R. J.; Clarke, N.; Winey, K. I. *Macromolecules* **2013**, *46*, 5345.
10. Li, W.; Liu, X.; Qian, G.; Deng, *J. Chem. Mater.* **2014**, *26*, 1948.
11. Quintana, M.; Vazquez, E.; Prato, M. *Acc. Chem. Res.* **2012**, *46*, 138.
12. Hu, W.; Zhan, J.; Wang, X.; Hong, N.; Wang, B.; Song, L.; Stec, A. A.; Hull, T. R.; Wang, J.; Hu, Y. *Ind. Eng. Chem. Res.* **2014**, *53*, 3073.
13. Thomassin, J.-M.; Trifkovic, M.; Alkarmo, W.; Detrembleur, C.; Jérôme, C.; Macosko, C. *Macromolecules* **2014**, *47*, 2149.
14. Wang, J.; Hu, H.; Wang, X.; Xu, C.; Zhang, M.; Shang, X. *J. Appl. Polym. Sci.* **2011**, *122*, 1866.
15. Fan, D.-Q.; He, J.-P.; Tang, W.; Xu, J.-T.; Yang, Y.-L. *Eur. Polym. J.* **2007**, *43*, 26.
16. Gardea, F.; Lagoudas, D. C. *Compos. Part B* **2014**, *56*, 611.
17. Fan, D.; Liu, Y.; He, J.; Zhou, Y.; Yang, Y. *J. Mater. Chem.* **2012**, *22*, 1396.
18. Mylvaganam, K.; Zhang, L. *J. Phys. Chem. C* **2013**, *117*, 2817.
19. Bhuyan, S.; Sundararajan, S.; Andjelkovic, D.; Larock, R. *Tribol. Int.* **2010**, *43*, 831.
20. Huang, Y.; Zeng, M.; Ren, J.; Wang, J.; Fan, L.; Xu, Q. *Colloids Surf. A* **2012**, *401*, 97.
21. Yu, F.; Cai, H.; He, W.; Yang, W.; Xie, Z. *J. Appl. Polym. Sci.* **2010**, *115*, 2946.
22. Sahoo, S.; Palai, R.; Barik, S. K.; Katiyar, R. S. *J. Raman Spectrosc.* **2013**, *44*, 798.
23. Giambastiani, G.; Cicchi, S.; Giannasi, A.; Luconi, L.; Rossin, A.; Mercuri, F.; Bianchini, C.; Brandi, A.; Melucci, M.; Ghini, G.; Stagnaro, P.; Conzatti, L.; Passaglia, E.; Zoppi, M.; Montini, T.; Fornasiero, P. *Chem. Mater.* **2011**, *23*, 1923.
24. Hwang, J.; Shields, V. B.; Thomas, C. I.; Shivaraman, S.; Hao, D.; Kim, M.; Woll, A. R.; Tompa, G. S.; Spencer, M. G. *J. Cryst. Growth* **2010**, *312*, 3219.
25. Dresselhaus, M. S.; Jorio, A.; Souza Filho, A. G.; Saito, R. *Philos. Trans. R. Soc. A* **2010**, *368*, 5355.
26. Fang, M.; Wang, K.; Lu, H.; Yang, Y.; Nutt, S. *J. Mater. Chem.* **2009**, *19*, 7098.
27. Georgakilas, V.; Otyepka, M.; Bourlinos, A. B.; Chandra, V.; Kim, N.; Kemp, K. C.; Hobza, P.; Zboril, R.; Kim, K. S. *Chem. Rev.* **2012**, *112*, 6156.
28. Wang, S.; Yu, D.; Dai, L.; Chang, D. W.; Baek, J.-B. *ACS Nano* **2011**, *5*, 6202.
29. Park, J.; Yan, M. *Acc. Chem. Res.* **2013**, *46*, 181.
30. Yan, X.; Chen, J.; Yang, J.; Xue, Q.; Miele, P. *ACS Appl. Mater. Interfaces* **2010**, *2*, 2521.
31. Kiwi, J.; Nadtochenko, V. *Langmuir* **2005**, *21*, 4631.
32. Zhao, Y.; Seredych, M.; Zhong, Q.; Bandosz, T. J. *RSC Adv.* **2013**, *3*, 9932.
33. Kunimatsu, K.; Bae, B.; Miyatake, K.; Uchida, H.; Watanabe, M. *J. Phys. Chem. B* **2011**, *115*, 4315.
34. Qian, X.; Song, L.; Yu, B.; Wang, B.; Yuan, B.; Shi, Y.; Hu, Y.; Yuen, R. K. K. *J. Mater. Chem. A* **2013**, *1*, 6822.
35. Laoutid, F.; Bonnaud, L.; Alexandre, M.; Lopez-Cuesta, J. M.; Dubois, P. *Mater. Sci. Eng. R* **2009**, *63*, 100.
36. Gann, J. P.; Yan, M. *Langmuir* **2008**, *24*, 5319.
37. Liu, H.; Ryu, S.; Chen, Z.; Steigerwald, M. L.; Nuckolls, C.; Brus, L. E. *J. Am. Chem. Soc.* **2009**, *131*, 17099.
38. Hsiao, M. C.; Liao, S. H.; Yen, M. Y.; Liu, P. I.; Pu, N. W.; Wang, C. A.; Ma, C. C. *ACS Appl. Mater. Interfaces* **2010**, *2*, 3092.
39. Patole, A. S.; Patole, S. P.; Jung, S.-Y.; Yoo, J.-B.; An, J.-H.; Kim, T.-H. *Eur. Polym. J.* **2012**, *48*, 252.
40. Potts, J. R.; Dreyer, D. R.; Bielawski, C. W.; Ruoff, R. S. *Polymer* **2011**, *52*, 5.